Optics Letters

Ultrafast and ultrahigh-resolution optical vector analysis using linearly frequency-modulated waveform and dechirp processing

Shupeng Li,[1] Min Xue,[1,2,4] Ting Qing,[1] Changyuan Yu,[2] Lugang Wu,[3] and Shilong Pan[1,5]

[1]Key Laboratory of Radar Imaging and Microwave Photonics, Ministry of Education, Nanjing University of Aeronautics and Astronautics, Nanjing 210016, China
[2]Department of Electronic and Information Engineering, Hong Kong Polytechnic University, Hong Kong
[3]Suzhou LiuYaoSi Information Technologies Co., Ltd., Changshu 215500, China
[4]e-mail: xuemin@nuaa.edu.cn
[5]e-mail: pans@nuaa.edu.cn

Received 24 April 2019; revised 30 May 2019; accepted 30 May 2019; posted 4 June 2019 (Doc. ID 365836); published 26 June 2019

We propose and experimentally demonstrate an ultrafast and ultrahigh-resolution optical vector analyzer (OVA) using linearly frequency-modulated (LFM) waveform and dechirp processing. An optical LFM signal, achieved by modulating an electrical LFM signal on an optical carrier via carrier-suppressed optical single-sideband (OSSB) modulation, is separated into two portions. One portion (denoted as the reference signal) directly goes through the reference path, and the other (denoted as the probe signal) undergoes magnitude and phase changes by an optical device under test (DUT) in the measurement path. After balanced photodetection, the reference signal and the probe signal are mixed to perform a dechirp operation. A relatively low-frequency electrical signal is generated, which can be sampled by a low-speed analog-to-digital converter. As a result, the frequency responses of the DUT can be extracted at a high speed by post digital signal processing. Thanks to the large chirp rate of the electrical LFM signal and the dechirp processing, the proposed LFM-based OVA enables ultrafast measurement speed and ultrahigh frequency resolution. We perform an experiment in which a narrowband tunable optical filter is characterized. The measurement speed reaches 1 ns/point, and the frequency resolution is 1.6 MHz.

https://doi.org/10.1364/OL.44.003322

Optical spectral response measurement is indispensable for the development and fabrication of optical components and photonic integrated circuits (PICs). Previously, to measure the magnitude, phase, and polarization responses, optical vector analyzers (OVAs) based on the interferometry method [1] or the modulation phase-shift approach [2] were developed. However, limited by the poor stability and low wavelength repeatability of tunable laser sources (TLSs), the frequency resolution is usually too low to observe the fine frequency responses of the optical components such as high-Q optical resonators [3,4], ultranarrow fiber Bragg gratings, and high-fineness PICs [5].

To achieve the high-resolution optical vector analysis, OVAs based on microwave photonics (MWP) were proposed and established [6–13], wherein the resolution of the measurement is improved by converting the frequency sweeping in the electrical domain into the optical domain via electrical-to-optical conversion. Benefitting from the high-resolution electrical frequency sweeping, the MWP-based OVAs theoretically have a sub-hertz resolution, and a frequency resolution of 334 Hz was experimentally achieved [8]. To make the MWP-based OVAs gaining ground in optics and photonics, many efforts have been devoted to the improvement of accuracy, dynamic range, measurement bandwidth, etc. A key problem associated with the MWP-based OVAs is the relatively slow measurement speed, as the responses at different frequencies are point-by-point measured. In particular, ultrahigh-resolution and broadband measurement require a large number of the measurement points and long-time post signal processing, which make the measurement time-consuming. In order to achieve fast measurement, an OVA based on optical channel estimation (OCE) was proposed and realized [14–16], which obtains the frequency responses by comparing two orthogonal frequency division multiplexing (OFDM) signals before and after an optical device under test (DUT). The responses at different frequencies are simultaneously measured, and a frequency resolution of 0.732 MHz is experimentally achieved. However, a high-speed analog-to-digital converter (ADC) is required for direct sampling of the OFDM signals, which has a low resolution and causes a small dynamic range. Moreover, the OCE-based OVAs suffer from nonlinear errors, because the OFDM signals have multiple frequency components at the same time.

In this Letter, we propose an OVA using linearly frequency-modulated (LFM) waveform and dechirp processing. In the proposed LFM-based OVA, an optical LFM signal is achieved by modulating an electrical LFM signal on an optical carrier via a carrier-suppressed optical single-sideband (OSSB) modulator. Different from the OFDM signal used in Refs. [14–16], LFM signal has only one frequency value at any given time, which is immune to nonlinear errors. In addition, the wideband LFM signal can support dechirp processing in the optical domain. Therefore, a low-speed photodetector and ADC are sufficient for the receiver, which enables a large dynamic range. In this work, the dechirp operation is performed by an MZI interferometer and a balanced detector. In an experiment, we measure a narrowband tunable optical filter with a frequency resolution of 1.6 MHz using the proposed OVA. Benefitting from the large chirp rate (1600 THz/s) of the LFM signal, the measurement with a bandwidth of 14.6 GHz takes only 10 μs, corresponding to 1 ns/point.

The schematic diagram of the proposed LFM-based OVA is shown in Fig. 1. An optical carrier from a TLS is fiber-coupled to a carrier-suppressed OSSB modulator, wherein the optical carrier is modulated by an electrical LFM signal from an electrical signal generator. After being amplified by an erbium-doped fiber amplifier (EDFA), the optical field of the signal can be written as

$$E_o(t) = E_o \exp[i \cdot (\omega_c t + \pi k t^2)] \qquad 0 \le t \le T, \tag{1}$$

where E_o is the complex amplitude, ω_c is the frequency of the optical carrier, k is the chirp rate of the electrical LFM signal, and T is the pulse width of the electrical LFM signal. Accordingly, the instantaneous optical frequency is

$$\omega_o(t) = \omega_c + 2\pi k t. \tag{2}$$

Then the optical signal is divided into two portions. One portion transmits through an optical DUT. The instantaneous optical frequency of the propagated optical signal can be given by

$$\omega_d(t) = \omega_c + 2\pi k\{t - \tau_1 - GD[\omega_d(t)]\}, \tag{3}$$

where τ_1 is the delay of the measurement path and $GD(\omega)$ is the group delay response of the DUT. Accordingly, the propagated optical signal can be expressed as

$$E_d(t) = E_d A[\omega_d(t)] \exp\left[i \cdot \int \omega_d(t) \mathrm{d}t\right], \tag{4}$$

where E_d is the complex amplitude of the optical signal injected into the DUT, $A(\omega)$ is the magnitude response of the DUT, and $\tau_1 + GD(\omega_c) \le t \le \tau_1 + T + GD(\omega_c + 2\pi k T)$.

Commonly, $GD(\omega)$ can be described as $GD(\omega) = \tau_d + gd(\omega)$, where τ_d is a constant, and $gd(\omega)$ is a term that varies with frequency. According to (3), the differential of ω_d is

$$d\omega_d = 2\pi k \cdot dt - 2\pi k \cdot d[gd(\omega_d)]. \tag{5}$$

When multiplying it by $gd(\omega_d)$ and performing the integral, (5) becomes

$$\theta[\omega_d(t)] = \int 2\pi k \cdot gd[\omega_d(t)] \cdot \mathrm{d}t - \pi k \cdot gd^2[\omega_d(t)]. \tag{6}$$

Considering that the value of k is 1600 THz/s in our experiment, $\pi k \cdot gd^2(\omega)$ will not exceed 0.00503 radians if the absolute value of $gd(\omega)$ is less than 1 ns. Therefore, $\pi k \cdot gd^2(\omega)$ is very small and can be ignored. With (3) and (6), (4) can be simplified to

$$\begin{aligned} E_d(t) = {} & E_d A[\omega_d(t)] \exp\{-i \cdot \theta[\omega_d(t)]\} \\ & \cdot \exp\{i \cdot [\omega_c(t - \tau_1 - \tau_d) + \pi k (t - \tau_1 - \tau_d)^2]\}. \end{aligned} \tag{7}$$

The other portion serves as the reference signal after being delayed by an optical fiber. The delayed optical signal is written as

$$E_r(t) = E_r \exp\{i \cdot [\omega_c(t - \tau_0) + \pi k (t - \tau_0)^2]\}, \tag{8}$$

where E_r is the complex amplitude of the reference signal, τ_0 is the delay of the reference path, and $\tau_0 \le t \le \tau_0 + T$. By combining the two optical signal and then performing balanced photodetection, a photocurrent carrying the transmission function of the DUT is obtained, which is

$$\begin{aligned} i_{\mathrm{BPD}}(t) &= \eta_1 |E_d(t) + i \cdot E_r(t)|^2 - \eta_2 |i \cdot E_d(t) + E_r(t)|^2 \\ &= (\eta_1 - \eta_2)(|E_d(t)|^2 + |E_r(t)|^2) \\ &\quad + 2(\eta_1 + \eta_2) \mathrm{Re}[i \cdot E_d(t) E_r^*(t)], \end{aligned} \tag{9}$$

where η_1 and η_2 are the responsivity of the two photodetectors in the balanced photodetector (BPD), respectively. As the ADC only responds to the AC term of the generated photodetector, the useful photocurrent is

$$i_{\mathrm{ADC}}(t) = 2(\eta_1 + \eta_2) \mathrm{Re}[i \cdot E_d(t) E_r^*(t)]. \tag{10}$$

To eliminate the influence from the measurement system, a normalization calibration is performed, wherein the two test ports are directly connected. The propagated signal delayed by the measurement path can be written as

$$E_s(t) = E_d \exp\{i \cdot [\omega_c(t - \tau_1) + \pi k (t - \tau_1)^2]\}. \tag{11}$$

Thus, the frequency responses of the measurement system are obtained:

$$i_{\mathrm{sys}}(t) = 2(\eta_1 + \eta_2) \mathrm{Re}[i \cdot E_s(t) E_r^*(t)]. \tag{12}$$

According to (10) and (12), the accurate magnitude and phase responses can be achieved:

$$\begin{aligned} H_{\mathrm{DUT}}(\omega_d) &= \frac{i_{\mathrm{ADC}} + i \cdot \hat{i}_{\mathrm{ADC}}}{i_{\mathrm{sys}} + i \cdot \hat{i}_{\mathrm{sys}}} \\ &= A(\omega_d) \exp\{-i \cdot [\omega_d \tau_d + \theta(\omega_d) + C]\}, \end{aligned} \tag{13}$$

where C is a constant, $\hat{i}_{\mathrm{ADC}}$ and $\hat{i}_{\mathrm{sys}}$ are the Hilbert transform of i_{ADC} and i_{sys}, respectively.

An experiment based on the setup shown in Fig. 1 is carried out. A TLS (Agilent N7714A) with a linewidth of less than 100 kHz generates an optical carrier, which is modulated at a carrier-suppressed OSSB modulator composed of a high-speed Mach–Zehnder modulator (MZM) and an optical tunable bandpass filter (Yenista XTA-50 Ultrafine). A modulator bias controller is used to keep the MZM biased at the

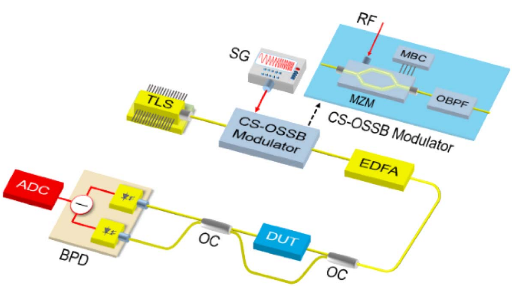

Fig. 1. Schematic diagram of the proposed LFM-based OVA. TLS, tunable laser source; CS-OSSB, carrier-suppressed optical single-sideband; SG, signal generator; EDFA, erbium-doped fiber amplifier; OC, optical coupler; DUT, device under test; BPD, balanced photodetector; ADC, analog-to-digital converter; MZM, Mach–Zehnder modulator; OBPF, optical band-pass filter; MBC, modulator bias controller.

minimum transmission point. An arbitrary waveform generator (AWG, Keysight M9502A) with a bandwidth of 26 GHz is employed to produce an electrical LFM signal with a chirp rate of 1600 THz/s, which works at a sampling rate of 64 GS/s. The start frequency and stop frequency are set to 10 and 26 GHz, respectively, and the pulse width of the electrical LFM signal is 10 μs. The generated optical LFM signal is amplified by an EDFA to 5 dBm. A narrowband tunable optical filter (TeraXion TFN-1550.12-N2-IL6-20-C1P-C) with a 3 dB bandwidth of 2.1 GHz is used as the DUT. A switchable gain balanced amplified photodetector (THORLABS PDB450C-AC) with a 3 dB bandwidth of 150 MHz is inserted to convert the optical signal into a photocurrent. A real-time oscilloscope (Agilent DSOX92504A) is used to sample the photocurrents from the BPD, which works at a sampling rate of 1 GS/s.

Figure 2 shows the optical spectrum of the carrier-suppressed OSSB signal when an RF signal with a frequency of 10 GHz is applied. As can be seen, due to the nonlinearity of the MZM, high-order sidebands can be observed, which is about 20 dB smaller than the desired sweeping sideband (i.e., the −1st-order sideband). Thus, the powers of the components beat by the high-order sidebands from the measurement path and the reference path are 40 dB lower than those of the component beat by the desired sidebands. Moreover, the beat note of the sweeping sidebands have the fundamental frequency, while the beat notes of the high-order sidebands are high-order harmonics, so they can be distinguished easily in the frequency domain. As a result, the components generated by the high-order sidebands can be further suppressed by digital filtering in the post-signal processing stage, by which the proposed LFM-based OVA can be considered to be immune to the measurement errors induced by the high-order sidebands. Based on the above analysis, the measurement errors are mainly induced by the +1st-order sideband, since the beat note has the same frequency as that of the desired −1st-order sideband. Therefore, a sideband suppression ratio (SSR) of the generated carrier-suppressed OSSB signal is of critical importance. Thanks to the sharp slope edges of the tunable optical bandpass filter (typical 800 dB/nm), the +1st-order sideband is well suppressed. As illustrated in Fig. 2, the SSR is 48.82 dB, which indicates that the power of the component beat by the sweeping sidebands is 97.64 dB larger than the undesired signal. Thus, the proposed LFM-based OVA could have a high accuracy.

Figure 3 shows the magnitude and phase responses of a narrowband tunable optical filter measured by the proposed LFM-based OVA, the ODSB-based OVA [11], and a commercial instrument (APEX AP2040C). Limited by the delay between

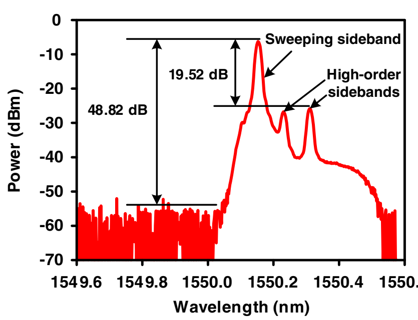

Fig. 2. Optical spectrum of the generated carrier-suppressed OSSB signal when a 10 GHz RF signal is applied.

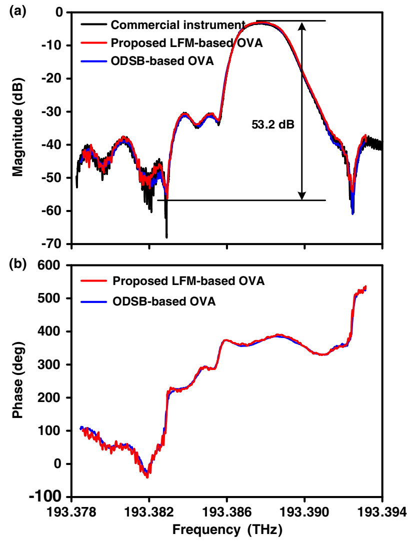

Fig. 3. (a) Magnitude and (b) phase responses of a narrowband tunable optical filter measured by the proposed LFM-based OVA, the ODSB-based OVA, and a commercial instrument.

the measurement path and reference path, the practical measurement range is 14.6 GHz, which is smaller than the 16 GHz frequency range of the electrical LFM signal. As can be seen from Fig. 3(a), the magnitude responses measured by the three methods, which overlap and have the same ups and downs coincide well. Benefitting from the digital bandpass filter, the signal-to-noise ratio of the desired fundamental frequency signal is greatly improved. Therefore, the magnitude response measured by the proposed LFM-based OVA has a small fluctuation. The maximum insertion loss of the measured magnitude response shown in Fig. 3(a) is about 50 dB. Considering that the measurable magnitude response with a 20 dB gain is measurable, a dynamic range of 70 dB is available for the experimentally implemented setup. If a high-resolution ADC (e.g., ADI AD9690) is used, the dynamic range can be further improved.

As shown in Fig. 3(b), the phase responses measured by the proposed LFM-based OVA and the ODSB-based OVA also agree well with each other. It should be noted that the phase fluctuation is obtained from the phase response measured by the proposed LFM-based OVA, because the practical laser source always has phase noise (e.g., the optical phase fluctuation), which appears as a linewidth of the laser source. By utilizing the model of the frequency-modulated continuous-wave (FMCW) interferometer [17], the probability density function of the phase fluctuation is given by

$$f(\Delta\phi) = \frac{1}{2\pi\sqrt{\Delta f \Delta\tau}} e^{-\frac{\Delta\phi^2}{4\pi\Delta f \Delta\tau}}, \quad \textbf{(14)}$$

where $\Delta\phi$ is the phase difference during a time period $\Delta\tau$ of a laser source with a linewidth of Δf. In the experiment, the linewidth is 100 kHz, and the time period is about 43.75 ns according to the delay difference between the measurement path and reference path. Hence, as shown in Fig. 4, the probability density of the phase fluctuation for the proposed LFM-based OVA can be achieved. As can be seen, the phase fluctuation distributes within ±10 deg, which agrees

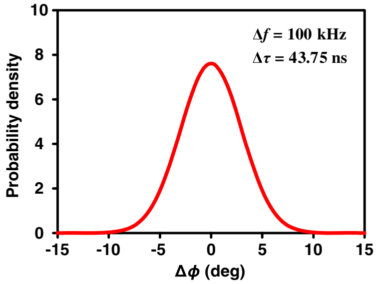

Fig. 4. Probability density of the phase fluctuation for the implemented measurement setup.

well with the measurement result. If a narrow linewidth laser source is adopted, the phase fluctuation can be reduced.

In addition, it takes only 10 μs for a measurement due to the narrow pulse width of the optical LFM signal. Benefitting from the short measurement time, the proposed LFM-based OVA would be insensitive to the temperature variation and mechanical vibration. Since the measurement time is 10 μs, the theoretical resolution can reach 100 kHz. Thanks to the linear time-frequency relationship of the LFM signal, the frequency resolution of the proposed LFM-based OVA would be the bandwidth of the signal divided by the total sampling points. Therefore, in such a short measurement time, the proposed LFM-based OVA still obtains a frequency resolution as high as 1.6 MHz, i.e., 16 GHz/(1 GS/s × 10 μs). To ensure the accuracy of the frequency response measurement, the sampling interval is required to be less than the group delay variation of the DUT. Therefore, the frequency resolution of the proposed OVA is determined by the chirp rate of the electrical LFM signal and the maximum group delay variation of the DUT, which can be described as

$$f_{\text{resolution}} \geq \frac{f_{\text{range}}}{\frac{1}{\max[gd(\omega)]} \cdot \frac{f_{\text{range}}}{k}} = k \cdot \max[gd(\omega)]. \tag{15}$$

In conclusion, an LFM-based OVA, featuring ultrafast measurement speed and ultrahigh frequency resolution, is proposed and experimentally demonstrated. The magnitude and phase responses of a narrowband tunable optical filter are successfully obtained during 10 μs, where the frequency resolution is 1.6 MHz, and the measurement range is 14.6 GHz. Only 1 ns is spent for measuring the frequency response at a frequency point showing the ultrafast measurement speed compared with the conventional ultrahigh-resolution OVAs. By employing an ultranarrow linewidth laser source, the phase fluctuation in the measured phase response can be reduced. The measurement bandwidth can be extended by adopting the channelized measurement technique based on optical frequency comb [18]. The proposed method may find application in fast characterization of optical components and PICs with ultrahigh resolution.

Funding. National Natural Science Foundation of China (NSFC) (61527820, 61705103); National Key R&D Program of China (2017YFF0106900); Jiangsu Provincial "333" Project (BRA2018042); Fundamental Research Funds for the Central Universities (NC2018005); Changshu Scientific and Technological Innovation and Entrepreneurship Leading Talents Program (CSRC1601).

REFERENCES

1. G. D. Vanwiggeren, A. R. Motamedi, and D. M. Barley, IEEE Photonics Technol. Lett. **15**, 263 (2003).
2. T. Niemi, M. Uusimaa, and H. Ludvigsen, IEEE Photonics Technol. Lett. **13**, 1334 (2001).
3. T. J. Kippenberg, R. Holzwarth, and S. A. Diddams, Science **332**, 555 (2011).
4. K. J. Vahala, Nature **424**, 839 (2003).
5. Y. Painchaud, M. Aubé, G. Brochu, and M. J. Picard, in *Advanced Photonics & Renewable Energy* (OSA, 2010).
6. S. Pan and M. Xue, J. Lightwave Technol. **35**, 836 (2017).
7. M. Sagues and A. Loayssa, Opt. Express **18**, 17555 (2010).
8. T. Qing, S. Li, Z. Tang, B. Gao, and S. Pan, "Optical vector analysis with attometer resolution, 90-dB dynamic range and THz bandwidth," arXiv:1902.06055 (2019).
9. W. Li, W. T. Wang, L. X. Wang, and N. Zhu, IEEE Photonics J. **6**, 1 (2014).
10. W. Jun, L. Wang, C. Yang, M. Li, N. Zhu, J. Guo, L. Xiong, and W. Li, Opt. Lett. **42**, 4426 (2017).
11. S. Liu, M. Xue, J. Fu, L. Wu, and S. Pan, Opt. Lett. **43**, 727 (2018).
12. M. Xue, S. Liu, and S. Pan, IEEE Photonics Technol. Lett. **30**, 491 (2018).
13. N. Kukharchyk, D. Sholokhov, O. Morozov, S. L. Korableva, J. H. Cole, A. A. Kalachev, and P. A. Bushev, Opt. Lett. **43**, 935 (2018).
14. X. Yi, Z. Li, Y. Bao, and K. Qiu, IEEE Photonics Technol. Lett. **24**, 443 (2012).
15. B. Guo, T. Gui, Z. Li, Y. Bao, X. Yi, J. Li, X. Feng, and S. Liu, Opt. Express **20**, 22079 (2012).
16. C. Jin, Y. Bao, Z. Li, T. Gui, H. Shang, X. Feng, J. Li, X. Yi, C. Yu, and G. Li, Opt. Lett. **38**, 2314 (2013).
17. S. Venkatesh and W. V. Sorin, J. Lightwave Technol. **11**, 1694 (1993).
18. M. Xue, S. L. Pan, C. He, R. H. Guo, and Y. J. Zhao, Opt. Lett. **38**, 4900 (2013).